23. M. H. Carr, *Icaurus* **56**, 476 (1983).
24. ______ *Water on Mars* (Oxford Univ. Press, xx, 1996), p. 229.
25. W. K. Hartmann *et al.*, *Basaltic Volcanism on the Terrestrial Planets* (Pergamon, New York, 1981), pp. 1049–1127.
26. G. Neukum and D. U. Wise, *Science*, **194**, 1381 (1976)
27. H. Y. McSween Jr. and R. P. Harvey, *Int. Geol. Rev.* **40**, 774 (1998).
28. P. H. Warren, *J. Geophys. Res.* **103**, 16759 (1998).
29. E. R. D. Scott, A. N. Krot, A. Yamaguchi, *Meteoritics* **33**, 709 (1998).
30. G. Turner, S. F. Knot, R. D. Ash, J. D. Gilmour, *Geochim. Cosmochim. Acta* **61**, 3835 (1997).
31. D. D. Bogard and D. H. Garrison, *Meteoritics* **34**, 451 (1999).
32. D. S. McKay *et al.*, *Science* **273**, 924 (1996).
33. D. York, *Can. J. Phys.* **44**, 1079 (1966).
34. M. Tatsumoto, R. J. Knight, C. J. Allègre, *Science* **180**, 1279 (1973).

35. We thank K. Manser for assistance with U-Pb analyses and D. C. Golden for assistance with P analyses. We also thank three anonymous reviewers for comments on the manuscript. This work was supported by NASA RTOP numbers 344-35-05-02 and 344-31-00-05 and was completed while L.E.B. held a National Research Council (Johnson Space Center) Research Associateship.

21 June 1999; 17 August 1999

The Gravity Field of Mars: Results from Mars Global Surveyor

David E. Smith,[1]* William L. Sjogren,[2] G. Leonard Tyler,[3] Georges Balmino,[4] Frank G. Lemoine,[1] Alex S. Konopliv[2]

Observations of the gravity field of Mars reveal a planet that has responded differently in its northern and southern hemispheres to major impacts and volcanic processes. The rough, elevated southern hemisphere has a relatively featureless gravitational signature indicating a state of near-isostatic compensation, whereas the smooth, low northern plains display a wider range of gravitational anomalies that indicates a thinner but stronger surface layer than in the south. The northern hemisphere shows evidence for buried impact basins, although none large enough to explain the hemispheric elevation difference. The gravitational potential signature of Tharsis is approximately axisymmetric and contains the Tharsis Montes but not the Olympus Mons or Alba Patera volcanoes. The gravity signature of Valles Marineris extends into Chryse and provides an estimate of material removed by early fluvial activity.

The gravity field of Mars reflects internal and external processes over several billion years, similar to the moon's. However, the magnitude of the variations on Mars indicates stress differences of about six times those in the Moon. The radio science investigation on the Mars Global Surveyor (MGS) mission (*1*) has developed global high-resolution gravitational field models (Fig. 1) for Mars from tracking data (Table 1) (*2, 3*) and provides new insight into the manner in which Mars has evolved through time in response to major impacts, surficial geological processes, and internal dynamics.

Tracking of the Mariner-9 and Viking-1 and -2 orbiters had limited coverage and lower accuracy data (*2, 4–6*) than MGS. The largest free-air gravity anomalies on Mars (Fig. 1A) associated with Olympus Mons and the Tharsis Montes (Ascraeus, Pavonis, and Arsia volcanoes) exceed 3000 mgal (*3*), more than an order of magnitude greater than those on Earth (*9*) for similar wavelengths (*10*). The substantial gravitational power (Fig. 2) is indicative of the ability of the planet's lithosphere to support large stresses associated with surface and subsurface loads (*11*). The thick lithosphere on Mars is a consequence of the more rapid loss of accretional and radiogenic heat from the martian interior as compared with Earth's. A striking feature of the field is the limited range of anomalies (± ~100 mgal) over a large fraction of the planet. Anomalies with substantial amplitudes are limited to the Tharsis, Isidis, and Elysium regions in the eastern and western hemispheres. A broad high of ~100 mgal in the midlatitude eastern hemisphere surrounds the Hellas basin and appears to be associated with material excavated from this structure (*12*).

Mars' gravitational potential, or areoid (*13*) (Fig. 1B), displays two hemispheric-scale quasi-circular features with a dynamic range of more than 2 km, an order of magnitude greater than that observed for Earth. The Tharsis Montes, Olympus Mons, Valles Marineris, and Isidis impact basin are resolved as individual gravitational anomalies in the areoid. Of particular note is the apparent circularity of the Tharsis areoid feature, in contrast to the complex topography of the region (*12*). The central portion of the Tharsis areoid encompasses the three Tharsis Montes in a single large anomaly and isolates Olympus Mons to the northwest. The Alba Patera volcanic construct also appears as a subtle feature separated from the main Tharsis areoid feature. The separation of Olympus and Alba from the main dome of Tharsis is similar to the topographic separation (*12*) and indicates that these prominent volcanic shields have distinctive source regions in the mantle that may explain the topography.

The zonal variation of gravity anomalies (Fig. 3) shows differences between the southern and northern hemispheres: the lack of gravity anomalies below major topographic features over most of the southern hemisphere, as well as substantial anomalies that lack topographic expression in the northern hemisphere. The smooth character of the gravity indicates that the topography in the southern latitudes is isostatically compensated much as are highland terrains on the moon (*14*).

The range of gravity variation from south to north (Fig. 3A) increases to as large as ~160 mgal. This suggests a latitude-dependent variation in compensation that may be associated with Mars' pole-to-pole 0.036° slope in topography (*12*) that might be explained by a systematic variation of crustal thickness with latitude. The longitudinal variation of gravity anomalies between latitudes 20°N to 75°N (Fig. 3B), and 20°S to 75°S (Fig. 3C) also emphasizes the difference between the two hemispheres. The uniform gravity field over most of the southern hemisphere in comparison with the much higher amplitude variation seen in the north is the antithesis of the topography, which is smooth in the north and rugged in the south. This points to a quantitative difference in the evo-

Table 1. Summary of spacecraft tracking data.

Spacecraft	Periapsis height (km)	Inclination (degrees)	Tracking
Mariner 9	1600	64	S-band Doppler
Viking 1	300, 1500	39, 55	S-band Doppler
Viking 2	300, 800, 1500	55, 75, 80	S-band Doppler
MGS	380, 263, 170	93	X-band Doppler, range

[1]Laboratory for Terrestrial Physics, National Aeronautics and Space Administration (NASA) Goddard Space Flight Center, Greenbelt, MD 20771, USA. [2]Jet Propulsion Laboratory, Pasadena, CA 91109, USA. [3]Center for Radio Astronomy, Stanford University, Stanford, CA 94035–4055, USA. [4]Group de Recherches de Geodesie Spatiales, Toulouse, France.

*To whom correspondence should be addressed: dsmith@tharsis.gsfc.nasa.gov

lution of the northern and southern hemispheres. The gravity data suggest a thin, strong lithosphere in the north and a thick, weak lithosphere in the south. Crustal magnetization measurements (*15*) suggest that the crust is older in the south than in the north, which implies that the south had a longer period of time available to achieve isostasy.

Gravity over the north polar region (Fig. 4A) reveals several positive anomalies that have no obvious correlation with topography (*16*). A combination of ice and crustal material has been proposed (*17*) to account for anomalies situated in the immediate vicinity of the north polar layered terrains. In contrast, the south polar region (Fig. 4B) shows a positive anomaly of ~200 mgal immediately over the pole, which could represent the load associated with the permanent ice cap. The lack of a comparable anomaly over the northern cap could indicate that the southern cap is younger and has not yet had sufficient time to adjust isostatically, or that the southern layered deposits contain a larger fraction of dust, thus constituting a greater gravitational load than in the north (*12*).

A possible explanation for the high-latitude northern hemisphere gravity anomalies, adjacent to and remote from the residual ice cap, is that they represent moderate-diameter (100 km) impact basins buried beneath the resurfaced northern hemisphere (*18*). The mass excesses implied by these positive anomalies may represent a combination of volcanic and sedimentary fill within the basin cavity and thinning of the northern hemisphere crust beneath the basin (*19*) that have not relaxed to an isostatic state (*20*).

Impact basins in Mars' southern hemisphere show primarily negative annular anomalies with a small central positive anomaly. Such signatures are characteristic of several basins on the moon (*14, 21*) that lack mare fill. The central anomaly probably represents mantle uplift, and the negative ring around it may represent a combination of uncompensated crustal thickening produced during the impact (*22*) and lithospheric flexure in response to the loading (*23*). The dominantly negative gravity signature is probably a consequence of a relatively thick crust that is able to withstand buoyancy forces from the mantle.

After Isidis, the largest impact-associated gravity anomaly (Table 2) is Utopia (Fig. 5A), which has been interpreted as an ancient basin on the basis of surface geology (*24*). Topographic data indicate that the basin is a quasi-circular depression ~1500 km in diameter (*25*), a factor of about 2 greater than originally proposed. Utopia's gravity anomaly is diffuse, occupying an area of $\sim 10^7$ km^2 with no clear center. The Utopia structure is buried beneath the northern hemisphere resurfacing, but the size of the depression and gravity anomaly suggest that the original basin could have been of a size comparable to that of Hellas (Fig. 5B) (*16*). However, these two massive structures appear in complete contrast gravitationally. Both appear to have readjusted isostatically, but Utopia was sub-

Table 2. Summary of prominent gravity anomaly amplitudes (*3, 7*). Lat., latitude; deg, degree; long., longitude.

Structure	Lat. (deg)	Long. (deg)	Anomaly (mgal)
Northern hemisphere			
Isidis	12°N	85°E	600
Utopia	45°N	110°E	350
Elysium	25°N	148°E	450
Olympus Mons	18°N	226°E	2750
Alba Patera	40°N	245°E	430
Ascraeus Mons	11°N	255°E	1380
Pavonis Mons	0°N	247°E	900
Southern hemisphere			
Arsia Mons	9°S	240°E	1350
Hellas	40°S	68°E	−150
Arygre	50°S	315°E	−140
Valles Marineris	5°S to 18°S	260°E to 330°E	−450

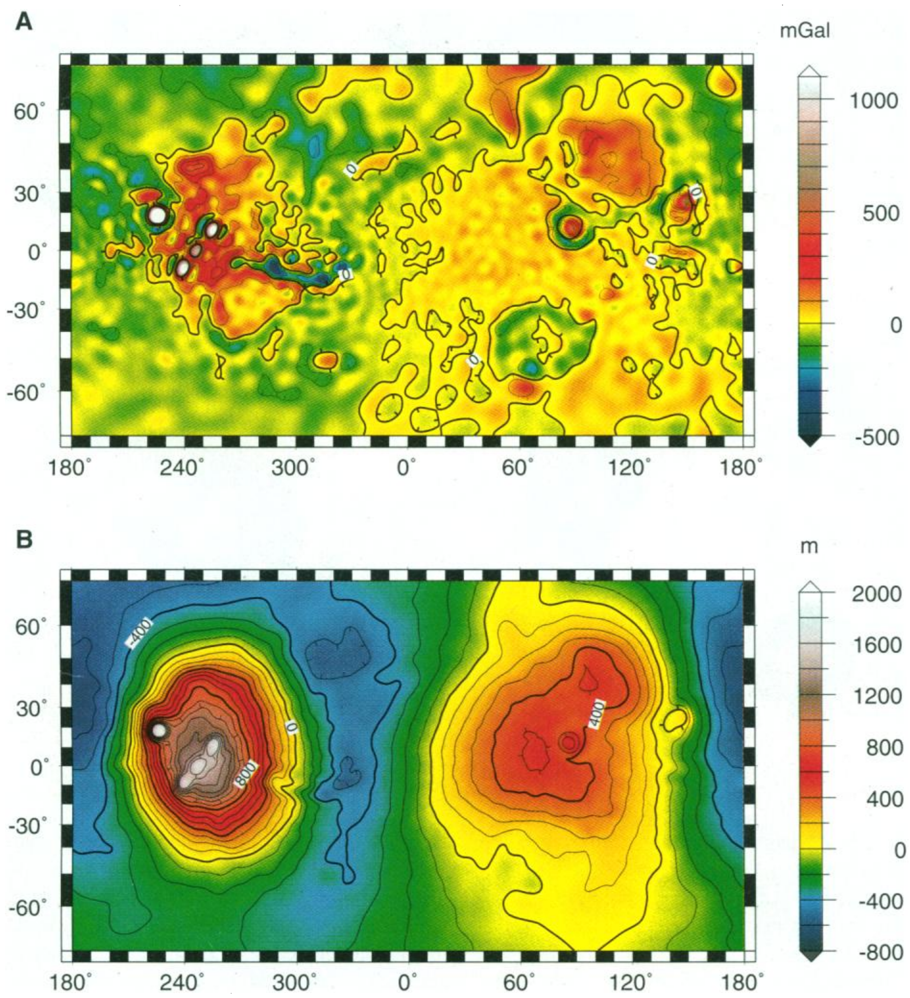

Fig. 1. (**A**) Free-air gravity (in milligals) for the mgs75b gravity model (*6*). (**B**) Areoid anomalies (in meters). The estimated hydrostatic contribution (95%) of the planetary flattening has been removed (*8*).

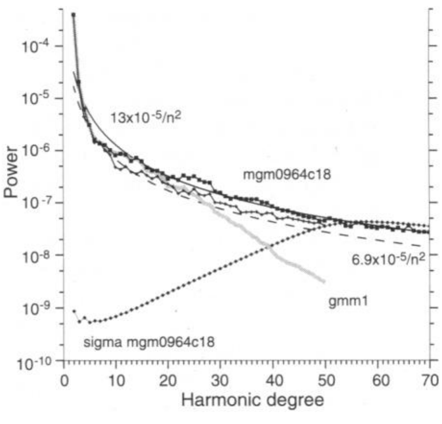

Fig. 2. Degree variances and error spectrum (*7*) and a power law (13×10^{-5} degree^{-2}) for comparison (not a fit to the data). Also shown are degree variances with Olympus Mons and the Tharsis volcanoes removed. The power in the spectrum approaches 6.9×10^{-5} degree^{-2}, close to that expected by scaling Earth's gravity field to Mars (*33*).

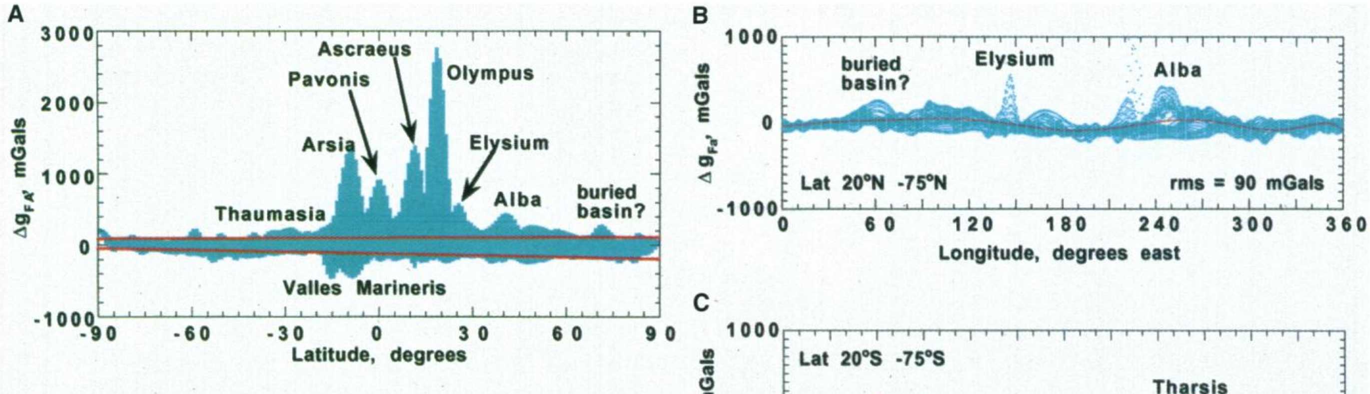

Fig. 3. (**A**) Zonal gravity anomalies (*7*). (**B**) Longitudinal gravity between latitudes 20°N and 75°N (*7*). (**C**) Longitudinal gravity between latitudes, 20°S and 75°S (*7*). The red lines in (A) illustrate the range of variation of anomalies.

sequently filled with material, which contributes to the gravitational mass excess. If the Utopia and Hellas structures were originally similar, the gravity field data may be able to shed light on the density of the material that has filled Utopia and by inference on the material of the northern plains.

Other than Utopia, the northern hemisphere lacks large (~1000 km) gravity anomalies that represent evidence for the large impact or impacts (*26*) proposed to explain the low elevation of the northern hemisphere relative to the south. If such basins existed, their geophysical signatures have been obliterated.

Other substantial gravity anomalies include the Isidis impact basin, the Elysium volcano-tectonic rise, and Olympus Mons. All show strong positive anomalies surrounded by negative annuli indicative of the flexural response of the lithosphere to surface or subsurface loads (*27*). The negative moat of Olympus is disrupted to the northwest because of a positive anomaly associated with the aureole deposits. The Tharsis Montes also show strong central positives and display evidence of surrounding gravity lows, but their close proximity to the center of Tharsis makes identification of these additional features less obvious. All five volcanoes deviate substantially from isostasy, indicating that they are relatively young and supported by a mechanically strong crust (*28*).

Valles Marineris shows a strong negative anomaly congruent with the topography (Fig. 6). The rift axis anomaly is the largest negative gravity feature on Mars and is due mostly to the mass deficit associated with the chasm (*29*), which has a depth of 11 km below the surrounding terrain at its lowest point (*12*). The canyons are flanked by gravity highs but the canyon system lacks a negative anomaly, broader than the rift, that is associated with upwelling of hot mantle material beneath active rifts on Earth

Fig. 4. (right) Polar stereographic plots of free-air gravity for the north (**N**) and south (**S**) polar regions (*7*). The plots extend from 70° to the poles. The color scale is the same as in Fig. 1A. **Fig. 5.** (below) Gravity of the Utopia (**A**) and Hellas (**B**) basins (*7*).

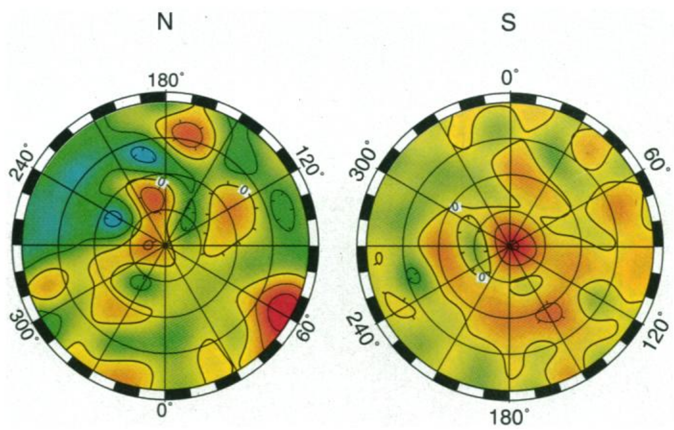

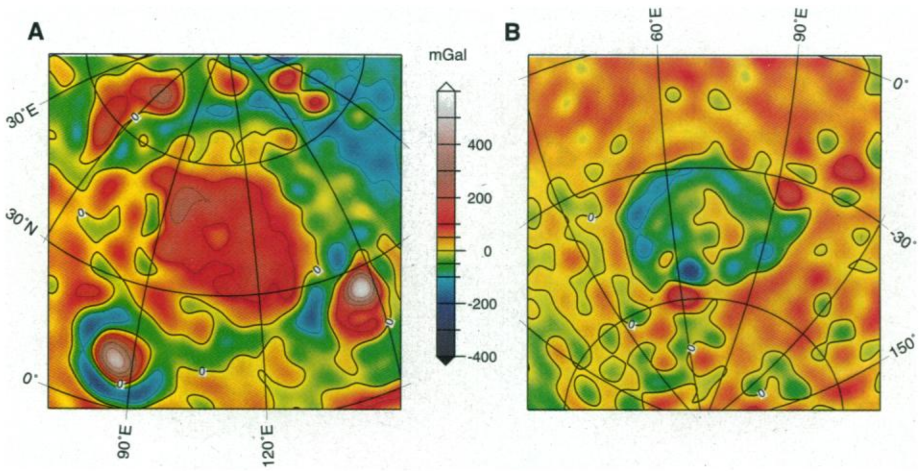

(*30*). The deviation of the canyon from isostatic compensation is consistent with its formation subsequent to Argyre and Hellas (*31*) and suggests that the martian lithosphere has not yet adjusted to its presence.

The negative anomaly of the central canyons can be traced into the Chryse outflow region and into the northern lowlands. Chryse was proposed to be the site of an ancient impact basin (*32*); however, the region lacks any mass anomaly displayed by other northern hemisphere impact basins, as well as any hint of a circular topographic depression (*12*). Instead, the mass deficiency implied by the Chryse anomaly (~200 mgal) may indicate the removal of >2 km of material by fluvial processes that carved the outflow channels early in martian history.

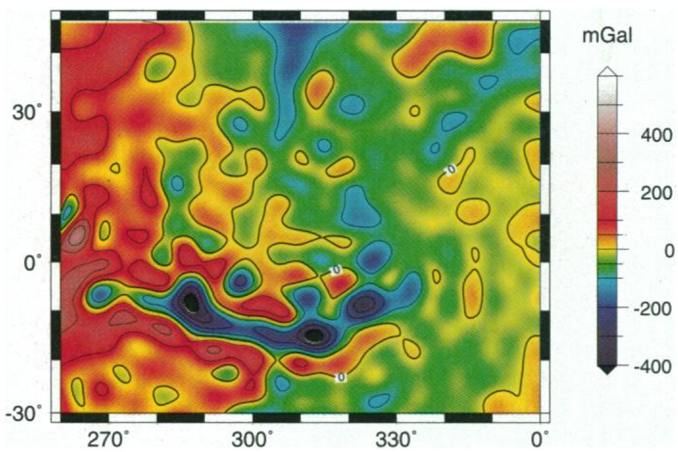

Fig. 6. Gravity of the Valles Marineris canyons system and Chryse outflow channels (*7*).

References and Notes

1. G. L. Tyler *et al.*, *J. Geophys. Res.* **97**, 7759 (1992); A. A. Albee, F. D. Palluconi, R. E. Arvidson, *Science* **279**, 1671 (1998).
2. Doppler radio tracking observations of MGS (primary) and selected Mariner 9 and Viking 1 and 2 data were used. MGS observations are "two-way" at 7.9 and 8.4 GHz. Mariner 9 and Viking were 2.1 and 2.3 GHz, respectively. The accuracy of MGS is better than 0.1 mm s^{-1} for an averaging time of 10 s.
3. Independent models were developed at NASA Goddard Space Flight Center (GSFC) and the Jet Propulsion Laboratory (JPL). The fields were solved (*33*) to degree and order 70 (*7*) and 75 (*6*), but are shown and interpreted only to degree and order 48, corresponding to a half-wavelength resolution of 220 km. Peak values of gravitational features depend on the effective resolution of the gravity model.
4. G. Balmino, B. Moynot, N. Vales, *J. Geophys. Res.* **87**, 9735 (1982); D. E. Smith *et al.*, *ibid.* **98**, 20871 (1993); A. S. Konopliv and W. L. Sjogren, "The JPL Mars gravity field, Mars50c, based upon Viking and Mariner 9 Doppler Tracking data," *JPL Publ. 95–5* (Jet Propulsion Laboratory, Pasadena, CA, 1995).
5. P. B. Esposito *et al.*, in *Mars*, H. H. Kieffer, B. M. Jakosky, C. W. Snyder, M. S. Matthews, Eds. (Univ. of Arizona Press, Tucson, 1992), pp. 209–248.
6. W. L. Sjogren, D. Yuan, A. S. Konopliv, *Eos* **80**, 204 (abstr.) (1999).
7. D. E. Smith, F. G. Lemoine, M. T. Zuber, *ibid.*, p. 204 (abstr.) (1999).
8. Gravity potential of the hydrostatic figure can be represented by even zonal harmonics. For Mars, about 95% of the degree 2 term is estimated to be due to the hydrostatic figure [W. A. Heiskanen and H. Moritz, *Physical Geodesy* (Freeman, New York, 1967); W. M. Folkner *et al.*, *Science* **278**, 1749 (1997); M. T. Zuber and D. E. Smith, *J. Geophys. Res.* **102**, 28673 (1997)]. The remaining 5% corresponds to nonhydrostatic contributions associated with surface processes and internal dynamics.
9. F. G. Lemoine *et al.*, "The development of the joint NASA GSFC and the National Imagery and Mapping Agency (NIMA) geopotential model EGM96," *NASA/TP-1998–206861* (1998).
10. Commission errors at the poles and the equator are ~10 mgal and ~20 mgal, respectively. The errors are larger in regions of major anomalies (Table 2), such as Olympus Mons, where the error is ~100 mgal.
11. D. L. Turcotte, R. J. Willemann, W. F. Haxby, J. Norberry, *J. Geophys. Res.* **86**, 3951 (1981).
12. D. E. Smith *et al.*, *Science* **284**, 1495 (1999).
13. The areoid is a surface of constant gravity potential on Mars. Areoid anomalies are deviations from a specified equipotential surface defined here as the potential of the mean equatorial radius of Mars of 3396.0 km.
14. M. T. Zuber, D. E. Smith, F. G. Lemoine, G. A. Neumann, *Science* **266**, 1839 (1994).
15. M. H. Acuña *et al.*, *ibid.* **284**, 790 (1999); J. E. P. Connerney *et al.*, *ibid.* **284**, 794 (1999).
16. M. T. Zuber *et al.*, *ibid.* **282**, 2053 (1998).
17. C. L. Johnson *et al.*, in preparation.
18. In early martian history (>4 billion years), volcanic material flooded the low northern hemisphere [M. H. Carr, *The Surface of Mars* (Yale Univ. Press, New Haven, CT, 1981)], and produced vast, smooth plains [D. E. Smith *et al.*, *Science* **279**, 1686 (1998)].
19. Modeling gravity and topography of lunar basins indicates that several are superisostatic, and estimated thickness of basaltic mare fill is inadequate to explain the magnitude of the central positive anomaly (*14, 22*) [H. J. Melosh, *Impact Cratering: A Geologic Process* (Oxford Univ. Press, New York, 1989)].
20. Where lithosphere viscosity decreases with depth, longer wavelength loads relax more rapidly than shorter wavelength loads.
21. S. R. Bratt, S. C. Solomon, J. W. Head, *J. Geophys. Res.* **90**, 12415 (1985); A. S. Konopliv *et al.*, *Science* **281**, 1476 (1998).
22. G. A. Neumann, M. T. Zuber, D. E. Smith, F. G. Lemoine, *J. Geophys. Res.* **101**, 16841 (1996).
23. G. A. Neumann and M. T. Zuber, *Lunar Planet. Sci. Conf.* **XXVIII**, 1713 (1997).
24. G. E. McGill, *J. Geophys. Res.* **94**, 2753 (1989).
25. M. T. Zuber *et al.*, *Geophys. Res. Lett.* **25**, 4393 (1998).
26. D. E. Wilhelms and S. W. Squyres, *Nature* **309**, 138 (1984); H. V. Frey, and R. A. Schultz, *Geophys. Res. Lett.* **15**, 229 (1988).
27. D. L. Turcotte and G. Schubert, *Geodynamics: Applications of Continuum Physics to Geological Problems* (Wiley, New York, 1982).
28. R. P. Comer, S. C. Solomon, J. W. Head, *Rev. Geophys.* **23**, 61 (1985); S. C. Solomon *et al.*, *Lunar Planet. Sci. Conf.* **XXIX**, 1389 (1998).
29. S. Anderson and R. E. Grimm, *J. Geophys. Res.* **103**, 11113 (1998).
30. A. M. C. Sengor and K. Burke, *Geophys. Res. Lett.* **5**, 419 (1978).
31. D. H. Scott and K. L. Tanaka, *U.S. Geol. Surv. Map I-1802-A* (1986); R. Greeley and J. E. Guest, *U.S. Geol. Surv. Map I-1802-B* (1987).
32. R. A. Schultz and H. V. Frey, *J. Geophys. Res.* **95**, 14175 (1990).
33. W. M. Kaula, *Theory of Satellite Geodesy, Applications of Satellites to Geodesy* (Blaisdell, Waltham, MA, 1966).

34. The data used in this study will be deposited with the NASA Planetary Data System (http://pds-geophys.wustl.edu/pds/) 1 October 1999. We gratefully acknowledge P. Priest, S. Abbate, S. Asmar, and M. Connally for the observations; G. Neumann, S. Fricke, and D. Yuan for data analysis; and R. Simpson and J. Twicken for data assessment and archiving. We thank the MGS spacecraft and operation teams at JPL and Lockheed-Martin Astronautics in the management of the MGS mission and M. Zuber for stimulating and helpful discussions regarding the interpretation. This investigation was supported by the NASA Mars Global Surveyor Project.

29 July 1999; accepted 8 September 1999

Sulfuric Acid on Europa and the Radiolytic Sulfur Cycle

R. W. Carlson,[1]* R. E. Johnson,[2] M. S. Anderson[1]

A comparison of laboratory spectra with Galileo data indicates that hydrated sulfuric acid is present and is a major component of Europa's surface. In addition, this moon's visually dark surface material, which spatially correlates with the sulfuric acid concentration, is identified as radiolytically altered sulfur polymers. Radiolysis of the surface by magnetospheric plasma bombardment continuously cycles sulfur between three forms: sulfuric acid, sulfur dioxide, and sulfur polymers, with sulfuric acid being about 50 times as abundant as the other forms. Enhanced sulfuric acid concentrations are found in Europa's geologically young terrains, suggesting that low-temperature, liquid sulfuric acid may influence geological processes.

Europa is unique among Jupiter's moons. It is differentiated (*1*) with an icy crust that may melt from tidal heating to produce a subsurface ocean (*2*). The surface may be young and renewed by solid state convection (*3*) or extrusion of solid or liquid material from below (*4*). Europa's surface exhibits bright, icy plains and younger, darker mottled terrain (*4*). Linear features with different morphologies crisscross the surface. These long (>1000 km), narrow (10 to 20 km) features often show bright central bands flanked by bands of darker material ("triple bands"). Because Europa is within Jupiter's energetic magnetosphere, the surface is subject to intense bombardment by high-energy plasma (e^-, H^+, O^{n+}, and S^{n+}) (*5–7*) that can alter the

[1]Jet Propulsion Laboratory, California Institute of Technology, Pasadena, CA 91109, USA. [2]Engineering Physics, School of Engineering and Applied Sciences, University of Virginia, Charlottesville, VA 22903–2442, USA.

*To whom correspondence should be addressed. E-mail: rcarlson@lively.jpl.nasa.gov